A&A 531, A14 (2011)
DOI: 10.1051/0004-6361/201016264

Astronomy & Astrophysics

Infrared-faint radio sources: a cosmological view

AGN number counts, the cosmic X-ray background and SMBH formation

P.-C. Zinn[1], E. Middelberg[1], and E. Ibar[2]

[1] Astronomical Institute, Ruhr-University Bochum, Universitätsstraße 150, 44801 Bochum, Germany
e-mail: zinn@astro.rub.de
[2] UK Astronomy Technology Centre, Royal Observatory, Blackford Hill, Edinburgh EH9 3HJ, UK

Received 6 December 2010 / Accepted 31 March 2011

ABSTRACT

Context. Infrared-faint radio sources (IFRS) are extragalactic emitters clearly detected at radio wavelengths but barely detected or undetected at optical and infrared wavelengths, with 5σ sensitivities as low as 1 μJy.
Aims. Spectral energy distribution (hereafter SED) modelling and analyses of their radio properties indicate that IFRS are consistent with a population of (potentially extremely obscured) high-redshift AGN at $3 \leq z \leq 6$. We demonstrate some astrophysical implications of this population and compare them to predictions from models of galaxy evolution and structure formation.
Methods. We compiled a list of IFRS from four deep extragalactic surveys and extrapolated the IFRS number density to a survey-independent value of (30.8 ± 15.0) deg^{-2}. We computed the IFRS contribution to the total number of AGN in the Universe to account for the cosmic X-ray background. By estimating the black hole mass contained in IFRS, we present conclusions for the SMBH mass density in the early universe and compare it to relevant simulations of structure formation after the Big Bang.
Results. The number density of AGN derived from the IFRS density was found to be ~310 deg^{-2}, which is equivalent to a SMBH mass density of the order of 10^3 $M_\odot$ Mpc^{-3} in the redshift range $3 \leq z \leq 6$. This produces an X-ray flux of 9×10^{-16} W m^{-2} deg^{-2} in the 0.5–2.0 keV band and 3×10^{-15} W m^{-2} deg^{-2} in the 2.0–10 keV band, in agreement with the missing unresolved components of the Cosmic X-ray Background. To address SMBH formation after the Big Bang we invoke a scenario involving both halo gas accretion and major mergers.

Key words. X-rays: diffuse background – radio continuum: galaxies – early Universe – galaxies: active

1. Introduction

Infrared-faint radio sources (IFRS) were first classified by Norris et al. (2006), who identified them as sources detected at 1.4 GHz using the Australia Telescope Compact Array (ATCA) that were absent from deep infrared images from the *Spitzer* Wide-area InfraRed Extragalactic (SWIRE) survey (Lonsdale et al. 2003). In the process of matching IR counterparts to radio sources from the Australia Telescope Large Area Survey (ATLAS), Norris et al. found a total of 22 radio sources to which no infrared counterpart could be reasonably identified in any of the observed *Spitzer* bands (3.6–24 μm), down to a sensitivity of $\sigma_{3.6\,\mu\mathrm{m}} = 1.0\,\mu$Jy. A similar result was obtained by Middelberg et al. (2008a) who, found 31 IFRS in the ELAIS-S1 at similar IR and radio sensitivities. A substantial fraction of these IFRS have flux densities of several mJy at 1.4 GHz, and some are even found at 20 mJy.

A first attempt to investigate the nature of the IFRS discovered in the ATLAS survey was undertaken by Norris et al. (2007), who observed two IFRS with Very Long Baseline Interferometry (VLBI), and detected one. They argued that IFRS are AGN-driven objects because the VLBI detection indicated a brightness temperatures in excess of 10^6 K. These high temperatures cannot be reached by thermal emission mechanisms, hence indicate non-thermal radio emission produced by an AGN. Middelberg et al. (2008b), also using VLBI observations, then confirmed that at least a fraction of the IFRS population must contain an AGN contributing to the total IFRS spectral energy distribution.

These results were complemented by Garn & Alexander (2008) who identified an IFRS population in the *Spitzer* extragalactic First Look Survey (xFLS). Modelling their spectral energy distributions (SEDs) with template SEDs from known objects to estimate IFRS redshifts, they found that the characteristics of IFRS resembled a variety of 3C sources redshifted to $2 \leq z \leq 5$. A more detailed SED analysis was presented by Huynh et al. (2010), who used new, very deep *Spitzer* data in the *Chandra* Deep Field South (CDF-S) field obtained during two *Spitzer* legacy programs, SIMPLE (Damen et al., in prep.) and FIDEL (PI: Dickinson). With a sensitivity of $\sigma_{3.6\,\mu\mathrm{m}} = 0.16\,\mu$Jy, the IR counterparts to two of the four investigated IFRS were identified. Furthermore, a faint optical counterpart ($V = 26.27$ AB-mag) to one of the IFRS was serendipitously identified within the GOODS HST/ACS imaging campaign (Giavalisco et al. 2004). A second IFRS located within the GOODS-South field was found to have no optical detection at all (implying $V > 28.9$ AB-mag), placing strong constraints on their SEDs. Huynh et al. also searched other deep multi-wavelengths data sets in the CDF-S for counterparts, in particular the *Chandra* 2 Ms source catalog (Luo et al. 2008), the GEMS HST imaging campaign (Rix et al. 2004), and the MUSYC catalog (Gawiser et al. 2006). These searches did not identify any counterparts in the X-ray or the optical/NIR regime. Modelling template SEDs to represent the radio and, if available, the IR and optical detections, Huynh et al. (2010) found that a 3C 273-like object can

reproduce the data when redshifted to $z = 2$ (IR-detection) and $z > 4$ (IR non-detection). The IR non-detections could not be explained by any template SED at redshifts smaller than ~4. These estimates constrain the redshift range of IFRS, placing at least a significant fraction of them at $z > 4$. On the other hand, given that none of the IFRS was detected at 24 μm, Huynh et al. (2010) conclude that IFRS fall well beyond the IR-radio correlation (see e.g. Appleton et al. 2004, whose $q_{24} = \log\left(S_{24\,\mu\mathrm{m}}/S_{20\,\mathrm{cm}}\right)$ parameter of 0.84 would imply a 24 μm flux density of 7 mJy for a typical IFRS with $S_{20\,\mathrm{cm}} = 1$ mJy). Hence, the IFRS radio emission cannot be explained by star-forming processes but is likely to be produced by AGN. This finding is supported by applying various calibrations of the 1.4 GHz luminosity as a star formation rate (SFR) tracer. For instance, the classical calibration by Bell (2003) gives star formation rates of around a million solar masses per year for a typical IFRS assumed to be located at $z = 4$, which is unphysical and hence suggests that the radio emission of IFRS cannot only be caused by star formation.

Using new radio data spanning 2.3 GHz to 8.6 GHz, Middelberg et al. (2011) analysed the radio properties of 18 ATLAS IFRS. They found unusually steep radio spectral indices with a median α of -1.4 ($S \propto \nu^{\alpha}$), and no spectral index flatter than -0.5. According to the z–α relation (e.g. Athreya & Kapahi 1998) that predicts steeper radio spectral indices at higher redshifts, these findings suggest that IFRS reside in the high-redshift Universe. Another result from Middelberg et al. is that the ratio of the radio to IR flux densities, $S_{20\,\mathrm{cm}}/S_{3.6\,\mu\mathrm{m}}$, is much larger for IFRS than for the general radio source population, and potentially exceeds 10^4, a value that is similar to that found in a sample of high redshift radio galaxies (HzRGs) by Seymour et al. (2007). These ratios and redshift dependencies are investigated in more detail by Norris et al. (2011). They suggest that IFRS have redshifts of $z \sim 5$ in the most extreme cases, because no 3.6 μm counterpart could be identified by stacking ultra-deep *Spitzer* observations at the location of 39 IFRS, reaching a stacked sensitivity of $S_{3.6\,\mu\mathrm{m}} \sim 0.2$ μJy.

In summary, the evidence from SED modelling, the very high $S_{20\,\mathrm{cm}}/S_{3.6\,\mu\mathrm{m}}$ ratios and, the steep spectral indices all suggest that IFRS are at high redshifts (at least $z > 2$) and contain AGN. In this paper, we present the implications of this population for the AGN number densities, the cosmic X-ray background (CXB), and structure formation models. Throughout this paper, we adopt a standard flat ΛCDM cosmology with $H_0 = 71\,\mathrm{km\,s^{-1}\,Mpc^{-1}}$ and $\Omega_{\mathrm{M}} = 0.27$.

2. Catalogue of known IFRS

In previous publications the selection criterion used to identify IFRS was simply "radio sources with no apparent IR counterpart". This is a rather loose definition, and we propose to replace this definition by the following two criteria:

- the ratio of radio to mid-IR flux, $S_{20\,\mathrm{cm}}/S_{3.6\,\mu\mathrm{m}}$, exceeds 500;
- the 3.6 μm flux density is smaller than 30 μJy.

The first criterion selects objects with extreme radio to IR flux ratios, making IFRS clear outliers from the IR-radio correlation. This encapsulates the requirement that IFRS are strong in the radio, but weak at infrared wavelengths. The second criterion ensures that the sources are at significant, cosmologically relevant, distances, to eliminate low-redshift radio-loud AGNs. For example, Cygnus A (with $S_{20\,\mathrm{cm}}/S_{3.6\,\mu\mathrm{m}} = 2 \times 10^5$) would be an IFRS based on its radio to IR flux ratio alone, but would be excluded by the 3.6 μm flux density cutoff.

Table 1. Summary of investigated surveys.

Survey Name	Area deg^2	3.6 μm limit μJy	20 cm limit μJy	IFRS number
ATLAS/CDF-S[a]	3.7	3.1	186	14
ATLAS/ELAIS-S1[a]	3.6	3.1	160	15
First Look Survey[b]	3.1	9.0	105	13
COSMOS[c]	1.1	1.0	65	13

Notes. The given sensitivity limits are all 5σ. [(a)] Radio from Norris et al. (2006) and Middelberg et al. (2008a), IR from Lonsdale et al. (2003). [(b)] Radio from Condon et al. (2003) and IR from Lacy et al. (2005). [(c)] Radio from Schinnerer et al. (2007) (only the inner part of the 20 cm map was searched for IFRS to assure a homogeneous noise level across the searched area) and IR from Sanders et al. (2007).

Alonso-Herrero et al. (2006) demonstrated that the near-to-mid-IR SEDs of galaxies dominated by AGN emission exhibit a power-law behaviour produced by re-emission from warm dust surrounding the AGN. They find that AGN can span a large range of optical-to-IR spectral slopes with a maximum $\alpha = -2.8$ but typically between -0.5 and -1.0. These values are similar to those observed in the radio. The k-corrections necessary to estimate the intrinsic $S_{20\,\mathrm{cm}}/S_{3.6\,\mu\mathrm{m}}$ values would produce a small difference with respect to the observed ones. It is evident that the first criterion preferably select IFRS if the spectral slope in the near-IR is steeper than in the radio, i.e. star-forming galaxies (with flatter spectra due to a dominant stellar emission) are scattered away from the sample. This weak dependency of $S_{20\,\mathrm{cm}}/S_{3.6\,\mu\mathrm{m}}$ on redshift suggests that IFRS are intrinsically extreme outliers of the IR-radio correlation. This implies that the second criterion is the most important one when selecting high-redshift sources using the dimming produced by cosmic distance.

Applying our criteria, we present in this paper a catalogue containing all IFRS found in the ATLAS/CDF-S (Norris et al. 2006) and ATLAS/ELAIS-S1 (Middelberg et al. 2008a) surveys, in the *Spitzer* extragalactic First Look Survey (xFLS, Condon et al. 2003), and in the COSMOS survey (Schinnerer et al. 2007). To date, this compilation is the most comprehensive list of IFRS, including 55 objects located in four individual surveys. The surveys were chosen not only because of their radio and IR coverage but also for the covered area. To minimise the effects of cosmic variance, only surveys of areas greater than 1 deg^2 were analysed. Cosmic variance can be a significant source of error when measuring density-related quantities especially in small survey fields. For example, the GOODS field was analysed for cosmic variance by Somerville et al. (2004). They found that for fields of the order of several 100 arcmin^2, such as GOODS, the error in number density estimates can range from 20% to 60% for strongly clustered sources. To avoid statistical errors introduced by cosmic variance in the estimated number counts, we excluded small area surveys. In particular, we omitted the deep surveys in the Lockman Hole East (Ibar et al. 2009) and Lockman Hole North (Owen & Morrison 2008). An overview of the surveys that we used is shown in Table 1.

The source selection process was as follows: a pre-selection of candidate sources was obtained by cross-matching radio and IR catalogues of each survey in two different ways. Radio sources showing a clear spatial extension, or those consisting of multiple components, were excluded from this pre-selection to prevent resolved AGN lobes entering the sample. All radio sources with a 3.6 μm counterpart within a 5″ radius were

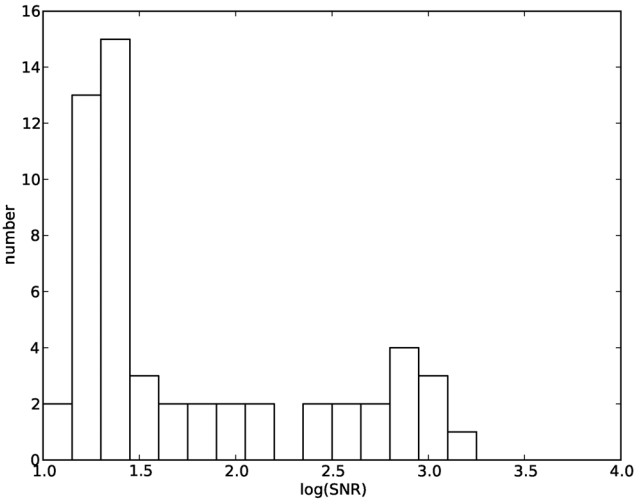

Fig. 1. Histogram of the *SNR* distribution at 20 cm for all IFRS presented in this paper. Note that the abscissa is logarithmic.

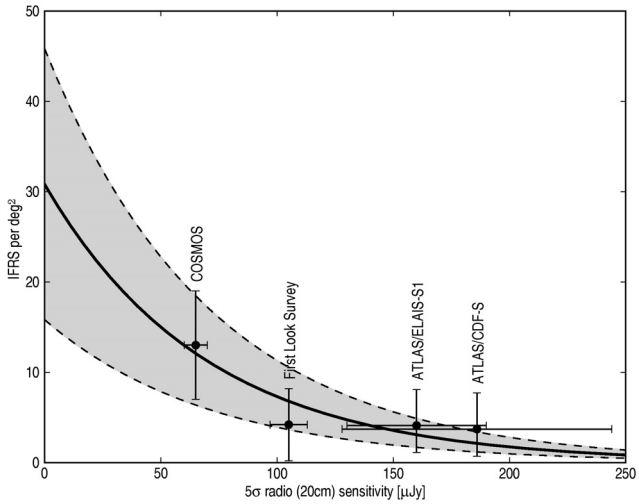

Fig. 2. Plot illustrating the extrapolation of IFRS surface density with respect to different radio sensitivities. The best fit (solid line) is given by $\lambda = (30.8 \pm 15.0)\exp\{(-0.014 \pm 0.006)5\sigma_{\rm radio}\}$, its quality in terms of χ^2/d.o.f. is 5.5, Pearson's correlation coefficient is $R^2 = 0.82$. The dashed curves that limit the shaded area correspond to fit functions representing the minimum and maximum values for the IFRS surface density with respect to the error of 15.0 given above.

selected and their $S_{20\,\rm cm}/S_{3.6\,\mu\rm m}$ ratio was calculated. For all radio sources that did not have a 3.6 μm counterpart within 5″, the 5σ detection limit of each survey as listed in Table 1 was chosen to provide a conservative upper limit to the 3.6 μm flux density. Hence the inferred $S_{20\,\rm cm}/S_{3.6\,\mu\rm m}$ is a lower limit, and is indicated as such in Table 2. A 5″ search radius for cross-matching the radio and 3.6 μm data ensures that at any redshift greater than $z = 0.5$, the corresponding linear distance is of the order of 30 kpc or more, hence exceeds the size of a large spiral galaxy. We then produced postage stamp images for the visual inspection of each candidate source, showing a grey-scale IR image centred on the radio position of the source with overlaid radio contours. These images were inspected by eye to determine whether the source is really an IFRS or whether the cross-matching process failed, e.g. because of an uncatalogued IR counterpart. We also addressed the problem of source blending caused by the different resolutions of the IR and radio images (*FWHM* of 1.66″ in the IRAC 3.6 μm channel, Fazio et al. 2004, compared to 11″ by 5″ in the ATLAS 1.4 GHz radio data). IFRS candidates with more than one plausible IR counterpart were rejected from the selection process, since $S_{20\,\rm cm}/S_{3.6\,\mu\rm m}$ could not be reliably determined. The final sample of 55 sources is listed in Table 2, and a histogram showing the distribution of radio *SNR* is shown in Fig. 1.

We note that the visual inspection of candidate sources helped us to maintain the rate of false detections (i.e., arising from imaging artefacts) at a minimum. The survey sensitivities in Table 1 were obtained by calculating the median of the rms at the source positions, as provided in the respective catalogues. We used this as a characteristic survey sensitivity rather than adopting the sensitivity limits given in the relevant publications because those limits were often related to the most sensitive regions of the observed areas, and thus were not representative.

3. IFRS densities

3.1. The sample

To derive an estimate of IFRS surface density, at least to within an order of magnitude, we analysed the four surveys quoted above. We used surveys with different sensitivities to extrapolate to the total surface density of IFRS in the Universe.

As shown in Table 1, the surface density of IFRS depends strongly on the sensitivity of the individual radio surveys, whereas the IR sensitivity seems to have little effect. The uncertainties in the individual measurements were obtained as follows: the error in radio sensitivity is the median absolute deviation (MAD) of the rms values at the position of the targets from a given radio survey. This measurement is insensitive to outliers and can characterise non-Gaussian distributions. Assigning errors to the measured IFRS surface densities is more complicated. We chose to follow a statistical *ansatz* claiming that there is an intrinsic IFRS surface density at the sensitivity limit of a given survey, $\lambda_{\rm intr}$, and the IFRS surface density that we actually measured for that survey, $\lambda_{\rm meas}$. Assuming a Poissonian distribution (because the IFRS surface density is always greater than zero and discrete), we determined the 95% confidence levels with which one would measure a surface density of $\lambda_{\rm meas}$, given the true surface density is $\lambda_{\rm intr}$. Because the Poisson distribution is asymmetric, this procedure yielded asymmetric errors for the surface densities.

To extrapolate the measured densities to an intrinsic IFRS surface density (which a radio observation with zero noise would yield), an exponential fit was used to model the measurements (shown in Fig. 2). We chose an exponential function for both a theoretical and practical reasons. The theoretical reason is that the function should be monotonic because there is no obvious reason why the IFRS surface density should peak around a certain sensitivity. The practical reason is that in our tests an exponential function yielded the best results with respect to a χ^2 test (χ^2/d.o.f. = 5.5). We thus define the extrapolated IFRS surface density as the value given by the y-axis intersect of the fit at (30.8 ± 15.0) IFRS/deg^2. We point out that this large error is real, underlining that this calculation has to be understood as an "order of magnitude" estimate only.

3.2. Motivation behind a redshift range for IFRS

To convert the surface density of IFRS to a space density, we assume that the bulk of IFRS populate the redshift range $3 \leq z \leq 6$.

Table 2. Catalog of known IFRS in both ATLAS fields (CDF-S and ELAIS-S1), the *Spitzer* extragalactic First Look Survey (xFLS), and the COSMOS field.

Survey	Identifier[a]	RA (J2000) h:m:s	Dec (J2000) d:m:s	$S_{1.4}$ GHz mJy	ΔS mJy	$S_{20\,cm}/S_{3.6\,\mu m}$	SNR	Flag[b]
ATLAS/ELAIS-S1	S1021	00:32:55.534	–43:16:27.15	16.1	0.81	575	19	
ATLAS/ELAIS-S1	S645	00:39:34.763	–43:42:22.58	5.46	0.4	780	13	
ATLAS/ELAIS-S1	S1018	00:29:46.525	–43:15:54.52	27.34	1.37	1012	19	
ATLAS/ELAIS-S1	S5	00:37:09.365	–44:43:48.11	15.16	0.76	1082	19	
ATLAS/ELAIS-S1	S1239	00:35:47.969	–42:56:55.40	23.19	1.16	1220	19	
ATLAS/ELAIS-S1	S66	00:39:42.452	–44:27:13.77	33.58	1.71	1865	19	
ATLAS/ELAIS-S1	S1156	00:36:45.856	–43:05:47.39	31.77	1.59	2888	19	
ATLAS/ELAIS-S1	S11	00:32:07.444	–44:39:57.18	1.67	0.014	557	14	
ATLAS/ELAIS-S1	S419	00:33:22.766	–43:59:15.37	1.67	0.010	557	15	
ATLAS/ELAIS-S1	S798	00:39:07.934	–43:32:05.83	7.79	0.43	>2597	18	M
ATLAS/ELAIS-S1	S749	00:29:05.229	–43:34:03.94	7.01	0.41	>2337	17	M
ATLAS/ELAIS-S1	S973	00:38:44.139	–43:19:20.43	9.14	0.46	>3046	19	M
ATLAS/ELAIS-S1	S427	00:34:11.592	–43:58:17.04	21.36	1.07	>7120	19	M
ATLAS/ELAIS-S1	S509	00:31:38.633	–43:52:20.80	22.2	1.11	>7400	20	M
ATLAS/ELAIS-S1	S201	00:31:30.068	–44:15:10.69	5.05	0.25	>1683	20	M
ATLAS/CDF-S	S114	03:27:59.894	–27:55:54.73	7.2	0.042	>2400	38	N
ATLAS/CDF-S	S194	03:29:28.594	–28:36:18.81	6.1	0.064	>2033	32	N
ATLAS/CDF-S	S703	03:35:31.025	–27:27:02.20	26.1	0.040	>8700	140	N
ATLAS/CDF-S	S292	03:30:56.949	–28:56:37.29	22.3	0.081	1842	119	
ATLAS/CDF-S	S649	03:34:52.846	–27:58:13.05	5.7	0.034	1838	30	
ATLAS/CDF-S	S618	03:34:29.754	–27:17:44.95	42.5	0.059	1660	228	
ATLAS/CDF-S	S574	03:33:53.279	–28:05:07.31	11.9	0.029	1091	63	
ATLAS/CDF-S	S94	03:27:40.727	–28:54:13.48	8.9	0.08	801	47	
ATLAS/CDF-S	S603	03:34:13.759	–28:35:47.47	13.2	0.039	709	70	
ATLAS/CDF-S	S713	03:35:37.525	–27:50:57.88	16.4	0.069	643	88	
ATLAS/CDF-S	S539	03:33:30.542	–28:54:28.22	9.1	0.070	640	48	
ATLAS/CDF-S	S265	03:30:34.661	–28:27:06.51	18.6	0.034	634	100	
ATLAS/CDF-S	S97	03:27:41.700	–27:42:36.61	4.3	0.033	614	23	
ATLAS/CDF-S	S520	03:33:16.754	–28:00:16.02	3.7	0.020	500	19	
xFLS	2009	17:18:56.948	+60:21:11.84	14.111	0.599	>1568	23	
xFLS	2779	17:22:30.252	+60:08:49.91	6.582	0.33	>731	19	
xFLS	2371	17:20:37.485	+60:14:42.80	5.34	0.228	~500	23	s
xFLS	1050	17:14:36.539	+59:44:56.44	4.058	0.174	~500	23	s
xFLS	1120	17:14:53.815	+59:43:29.28	3.685	0.158	~500	23	s
xFLS	478	17:11:48.526	+59:10:38.87	35.815	1.52	1831	23	uc
xFLS	600	17:12:25.462	+59:40:14.98	16.2	0.688	730	23	uc
xFLS	760	17:13:15.445	+59:03:02.66	2.47	0.11	>798	25	GA
xFLS	929	17:14:03.986	+59:53:17.54	2.42	0.10	>780	24	GA
xFLS	1050	17:14:36.539	+59:44:56.44	4.06	0.17	>1310	24	GA
xFLS	1120	17:14:53.815	+59:43:29.28	3.69	0.16	>1190	23	GA
xFLS	2398	17:20:46.548	+58:47:28.91	3.58	0.15	>1155	22	GA
xFLS	2928	17:23:15.537	+59:09:19.46	1.41	0.06	~500	21	GA,s
COSMOS	J095957.97+020109.7	09:59:57.97	+02:01:09.7	7.070	0.099	542	643	
COSMOS	J095959.16+014837.8	09:59:59.16	+01:48:37.8	9.600	0.110	886	873	
COSMOS	J100058.05+015129.0	10:00:58.05	+01:51:29.0	11.950	0.120	862	1195	
COSMOS	J100109.28+021721.7	10:01:09.28	+02:17:21.7	4.100	0.010	522	410	
COSMOS	J100120.06+023443.7	10:01:20.06	+02:34:43.7	10.796	0.112	1301	830	
COSMOS	J100209.06+021602.6	10:02:09.06	+02:16:02.6	6.136	0.068	515	558	
COSMOS	J100212.06+023134.8	10:02:12:06	+02:31:34.8	18.690	0.200	649	1699	
COSMOS	J100114.12+015444.3	10:01:14.12	+01:54:44.3	7.000	0.044	538	636	
COSMOS	J095803.21+021357.7	09:58:03.21	+02:13:57.7	25.302	0.264	1438	904	
COSMOS	J100129.35+014027.1	10:01:31.10	+01:40:18.0	6.330	0.597	1476	452	
COSMOS	J095908.87+013603.6	09:59:08.87	+01:36:03.6	6.484	0.085	500	359	
COSMOS	J100252.88+015549.7	10:02:25.88	+01:55:49.7	17.543	0.184	931	975	
COSMOS	J095838.01+013217.1	09:58:38.01	+01:32:17.1	4.577	0.095	509	254	

Notes. [a] The identifiers are given as in the original publications to ensure easy data handling. [b] s: uncertain IFRS (e.g. because the IR data is too shallow to yield a clear counterpart detection with reliable flux measurements, so that the error in IR flux is large). uc: uncataloged counterpart. GA: IFRS in Garn & Alexander (2008). M: IFRS in Middelberg et al. (2008a). N: IFRS in Norris et al. (2006).

There are several motivations for this choice: (i) it has been suggested by the SED modelling work described in Sect. 1 that most IFRS SEDs are inconsistent with template SEDs displaced to redshifts significantly less than $z = 4$; (ii) those few IFRS detected in 3.6 μm with this ultra-deep IR data are at at least $z = 2$ (see conclusions in Huynh et al. 2010); (iii) the radio to IR flux

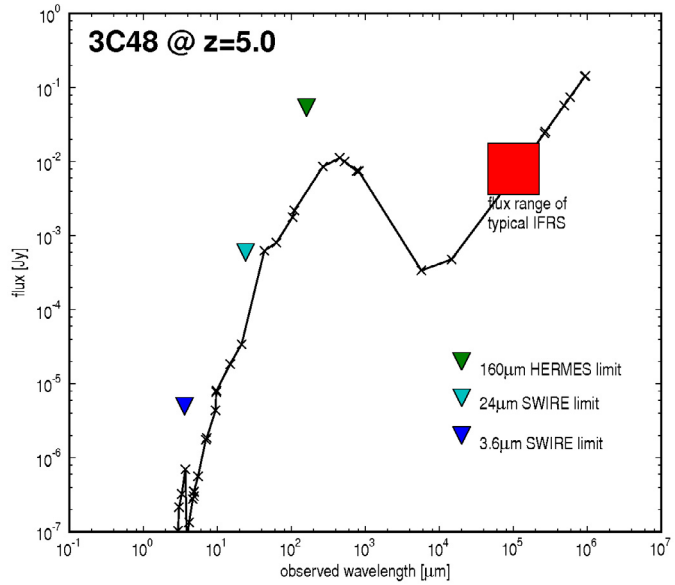

Fig. 3. The template SED of 3C 48, redshifted to $z = 5$, boosted in flux by a wavelength-independent factor of 5 and dimmed in the optical and NIR following a Calzetti et al. (2000) extinction law with $A_V = 1$. To emphasise that this SED is the one of an IFRS, we give the detection limits of the SWIRE survey described in Sect. 1 as well as the 160 μm limit of the planned *Herschel* Hermes survey. The radio spectral index of this SED corresponds to $\alpha = -1.4$.

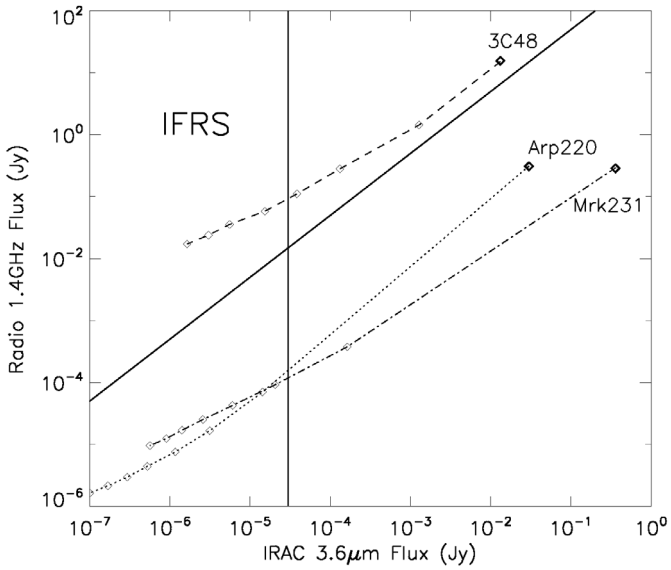

Fig. 4. Tracks showing the evolution of the radio and NIR luminosity of a 3C 48-like model with redshift. The redshift data points are given from right to left, starting with 3C 48's (and the other two comparative sources, Mrk 231 and Arp 220) intrinsic redshift (bold open square). The first thin open square from right indicates a redshift of $z = 1$, the next thin open square is equal to $z = 2$, and so on to $z = 7$. The vertical solid line indicates the IFRS NIR flux cutoff-criterion $S_{3.6\mu m} < 30\,\mu$Jy, the other solid line represents $S_{20\,cm}/S_{3.6\mu m} = 500$.

density ratios of IFRS are similar to those of the Seymour et al. (2007) HzRG sample, of which many sources have redshifts of 3 and above; (iv) IFRS have very steep radio spectra, which correspond to high redshifts according to the z–α relation. However, since there is a large intrinsic scatter in the z–α relation as e.g. given by Athreya & Kapahi (1998), we do not give quantitative redshift estimates based on this relation but employ it only as a qualitative hint. We therefore adopt $z = 3$ as a good compromise choice of lower limit for their redshift range.

The upper limit of $z = 6$ was chosen because of the scarcity of sources beyond this redshift, as has been found, e.g., in the Sloan Digital Sky Survey (SDSS; see e.g. Schneider et al. 2010; Fan et al. 2003). Whilst there is a significant number of quasars at redshifts of $z \sim 5$, their number rapidly decreases beyond $z \sim 6$, with only very few spectroscopically confirmed quasars having redshifts significantly greater than 6. Hence $z = 6$ is a reasonable upper limit for our estimates. The problem of obtaining redshift estimates for IFRS is discussed in more detail by Norris et al. (2011), who argue for redshifts as high as $z = 5$, using extrapolations of the $S_{20\,cm}/S_{3.6\mu m}$ ratios and 3.6 μm flux densities of typical IFRS.

Furthermore, to derive a theoretically motivated estimate of the minimum redshift for a typical IFRS, we extended the work of Huynh et al. (2010) who modelled the SEDs of IFRS using the known template SEDs of different astrophysical objects (see Sect. 1). We chose 3C 48 with an intrinsic redshift of 0.37 as a template. 3C 48 is an excellent IFRS candidate at higher redshifts because of its intrinsically high $S_{20\,cm}/S_{3.6\mu m}$ ratio; it therefore does not require huge amounts of obscuring dust to dim its observed NIR flux. We redshifted it to $z = 5$, boosted its flux by a constant factor of five and dimmed it in the optical in NIR wavelength range using a Calzetti et al. (2000) reddening law with $A_V = 1$. The resulting model SED can reproduce all observational characteristics of a typical IFRS. This result is illustrated in Fig. 3.

Using this model SED, we traced the evolution of its $S_{20\,cm}/S_{3.6\mu m}$ flux ratio as a function of redshift. We also included several radio spectral indices in our calculations to account for different radio components (e.g. bremsstrahlung, aged synchrotron, or flat AGN spectra) that could yield different radio spectral indices than the canonical $\alpha = -0.7$ ($S_\nu \propto \nu^\alpha$) for thermal synchrotron emission. Thus we account for the radio spectral indices being typically lower towards higher redshift.

The resulting plot (Fig. 4) shows that only beyond a redshift of $z = 3$ are 3C 48-like models able to reproduce the high $S_{20\,cm}/S_{3.6\mu m}$ flux ratios and the low 3.6 μm flux densities observed in IFRS. Our model calculations indicate that to reproduce the observed 1.4 GHz flux densities of a few mJy, steep spectral indices are preferred, which agrees with the results obtained by Middelberg et al. (2011).

3.3. The space density of IFRS and their SMBH

In our redshift range of $z = 3$–6, a solid angle of 1 deg^2 corresponds to a comoving volume of 21.5×10^6 Mpc^3 (Wright 2006), so the observed surface density of IFRS converts to an IFRS space density simply by dividing the extrapolated number density of IFRS per deg^2 by the comoving volume

$$n_{IFRS} = 1.44 \times 10^{-6}\,\mathrm{Mpc}^{-3}. \quad (1)$$

This space density can now be converted into a mass density of supermassive black holes (SMBHs) that power IFRS. However, simply adopting SMBH masses found in recent studies of large quasar surveys as described in Vestergaard et al. (2008) for the SDSS data release 3 (containing more than 15 000 quasars up to $z = 5$) would lead to an overestimate of SMBH masses because the limits of contemporary optical surveys prevent us from detecting high-z quasars with less than $M_{SMBH} \sim 10^8\,M_\odot$. The actual limit for the SDSS is about $3 \times 10^8\,M_\odot$ and is based on

the line width of broad emission lines in a quasar spectra used to determine $M_{\rm SMBH}$ from their equivalent width. When converted to optical luminosities, this corresponds to a lower limit of $M_i = -27.5$ for a $z = 4$ quasar. IFRS cannot be optically bright quasars, because they would have to contain large amounts of dust in their surroundings to maintain their IFRS nature, hence one has to lower the average SMBH mass found by Vestergaard et al. (2008), and Vestergaard & Osmer (2009) for high-redshift AGN of $\langle M_{\rm SMBH}\rangle \sim 10^9\,M_\odot$ (this value is supported by other work with much smaller quasar samples but more accurate methods for determining $M_{\rm SMBH}$, see e.g. Dietrich & Hamann 2004; Fine et al. 2008). For example, an SMBH radiating at its Eddington limit produces an unobscured $z = 4$ quasar with an apparent magnitude of 25.0 (a common limit for contemporary optical surveys carried out with space-based facilities), while having a mass of only $3.5 \times 10^6\ M_\odot$. Recent cosmological hydrodynamical simulations (e.g. Degraf et al. 2010) have shown that most SMBHs at $z = 5$ do not accrete at their Eddington limit but at a factor of approximately 5 to 10 times less. Nevertheless, observational evidence for the $L_{\rm Bol}/L_{\rm Edd}$ ratio indicates an accretion mechanism at $L_{\rm Bol}/L_{\rm Edd} = 1$ for the most distant quasars (Fan 2009). This discrepancy between theory and observations could be a selection effect in currently available observations because SMBHs that do not accrete at their Eddington limit would simply be too faint to be detected. Therefore we conclude that optical observations are unsuitable for estimating a typical SMBH mass for IFRS.

Another way of estimating the SMBH masses in IFRS are X-ray observations that are thought to be an efficient way of detecting large numbers of AGN. X-rays can leave the emission regions rather unabsorbed, and there is little contamination from other sources, such as stars. Given that no IFRS identified in the radio observations of the ELAIS-S1 field is detected in the corresponding X-ray survey by Puccetti et al. (2006), we can use this information to derive an upper limit for a SMBH. Using Eq. (5), a $4 \times 10^7\ M_\odot$ SMBH at $z = 4.5$ would just not be visible in the 0.5–2.0 keV band, given the detection limits of the Puccetti et al. (2006) survey of $5.5 \times 10^{-19}\,{\rm W\,m^{-2}}$[1]. Unfortunately, no IFRS is located in the CDF-S *Chandra* 2 Ms observation by Luo et al. (2008). The X-ray observations done within the COSMOS survey using XMM-*Newton* (Cappelluti et al. 2007, with a highest sensitivity of $7.2 \times 10^{-19}\,{\rm W\,m^{-2}}$ in the soft band), also did not yield a clear identification of an IFRS X-ray counterpart. We note that especially for the inner parts of the COSMOS X-ray image, the field is very crowded making the reliable detection of potentially very weak counterparts difficult. However, to provide some margin (to account for extinction, for example), we approximately double this value and therefore assume an *upper limit* for the mass for SMBHs in IFRS of $M_{\rm IFRS} \leq 10^8\,M_\odot$. Hence the mass density of SMBH in IFRS is

$$\rho_{\rm IFRS} \leq 1.4 \times 10^2\,M_\odot\,{\rm Mpc^{-3}}. \quad (2)$$

4. Implications

4.1. ... on AGN source counts

If we assume that IFRS contain AGN then we can more tightly constrain the total AGN number density and estimate their contribution to the total AGN population. To do that, one has to correct for not all AGN being radio sources, i.e., there being a population of faint AGN (due to an intrinsically low luminosity or because they are obscured by dust) of which we can identify only a fraction because of their radio emission. To estimate the total population of these faint AGN (fAGN hereafter), we adopt a value for the radio loud fraction derived by Jiang et al. (2007) of 10%, which has a scatter of only ±4% with increasing redshift. Hence the surface density of fAGN is of the order of $310\,{\rm deg^{-2}}$, and the space densities of fAGN and the SMBH mass density arising from this population are to be multiplied by ten. Since all further calculations must be regarded as "order of magnitude" estimates, we do not specify any errors. IFRS are a new class of object with particularly extreme radio properties, which may further increase the scatter in the relation found by Jiang et al. (2007), hence the error reported by Jiang et al. is likely to be too small for our calculations. Nevertheless, we adopt the main result by Jiang et al. (2007) that about one tenth of all AGN across the entire investigated redshift range ($z < 4$) are radio loud, and we infer the number density of fAGN traced by IFRS by simply correcting for this factor. Accordingly, the number density of fAGN in this redshift range and their SMBH mass density are, given the average mass of their SMBHs discussed above

$$n_{\rm fAGN} = 10 \cdot n_{\rm IFRS} = 1.44 \times 10^{-5}\,{\rm Mpc^{-3}}, \quad (3)$$

$$\rho_{\rm fAGN} = n_{\rm fAGN} \cdot M_{\rm IFRS} \leq 1.4 \times 10^3\,M_\odot\,{\rm Mpc^{-3}}. \quad (4)$$

On the basis of X-ray 0.5–2.0 keV band observations obtained with both XMM-*Newton* and *Chandra*, Hasinger et al. (2005) give a redshift-dependent space density of AGN for several X-ray luminosities. For their two faintest categories, they find values around $2 \times 10^{-5}\,{\rm Mpc^{-3}}$, which, given the many uncertainties in our estimate, is in very good agreement with the fAGN number density. Since X-ray surveys are thought to provide a reliable census of AGN (see e.g. Bauer et al. 2004, for an investigation of the completeness in the *Chandra* Deep Fields), this value should not exceed $5 \times 10^{-5}\,{\rm Mpc^{-3}}$ given the current X-ray survey sensitivity limits of $\sim 10^{-19}\,{\rm W\,m^{-2}}$. Nevertheless, there are a few bright radio sources that do not have an X-ray counterpart even in the 2 Ms *Chandra* exposure (e.g. Snellen & Best 2001) and actual number counts vary from survey to survey. For example, the XMM-*Newton* survey of the COSMOS field (Brusa et al. 2009) yields a space density of only $10^{-6}\,{\rm Mpc^{-3}}$ at $z = 4$, whilst the Gilli et al. (2007) model predicts a value that is four times higher. Therefore we propose to use the IFRS population to complement the number of X-ray-unidentified AGN in the Universe. For a concise review of AGN identification techniques, we refer to Mushotzky (2004).

We stress that comparing our results to other surveys must be done with exceptional care because the IFRS sample presented here may be biased, e.g. towards dusty sources. Further observations of a subsample of IFRS with the *Herschel* Space Observatory will clarify the dust content of these extreme objects.

For AGN at even higher redshifts ($z > 4$), Brandt & Hasinger (2005) give a lower limit to the surface density of AGN of 30–$150\,{\rm deg^{-2}}$. This value is of the same order of magnitude as our estimate of the fAGN surface density of $\sim 310\,{\rm deg^{-2}}$ (ten times the IFRS surface density). Considering that approximately half of these objects are likely to be situated at these high redshifts[2],

[1] For the convenience of the reader, we give the conversion factor between SI and old cgs units: $1\,{\rm W\,m^{-2}} \equiv 10^3\,{\rm erg\,s^{-1}\,cm^{-2}}$.

[2] With ultra-deep *Spitzer* data, Huynh et al. (2010) only found counterparts to two out of four IFRS, hence they conclude that this IR-undetected AGN exhibiting really extreme ratios of radio to infrared flux are located at similar extreme redshifts in the range of $z = 5$–6.

our estimates are in good agreement with the Brandt & Hasinger value.

4.2. ... on the cosmic X-ray background

Since no IFRS in the ELAIS-S1 field is detected as a discrete X-ray source by the corresponding XMM-*Newton* survey carried out by Puccetti et al. (2006), the question arises of where their X-ray radiation goes. We propose that the X-ray emission contributes to the cosmic X-ray background (CXB). Given the surface density of fAGN of ∼310 deg^{-2} and an average mass of their central SMBHs of $10^8\,M_\odot$, one can calculate their contribution. Following Dijkstra et al. (2004), an SMBH at its Eddington limit (we assume accretion at the Eddington limit because the general trend for high-mass SMBHs indicates this, see Willott et al. 2010) emits a flux density in the observer 0.5–2.0 keV band of

$$S_{\mathrm{SMBH}} = 3.8\times10^{-23}\left(\frac{M_{\mathrm{SMBH}}}{10^4\,M_\odot}\right)\left(\frac{f_{\mathrm{X}}}{0.03}\right)\left(\frac{10}{z_{\mathrm{AGN}}}\right)^{9/4}\ \mathrm{W\,m^{-2}}, \quad (5)$$

where f_{X} denotes the fraction of the total energy radiated in the observer 0.5–2.0 keV band, its value of 0.03 is taken from the template spectrum of Sazonov et al. (2004) and will be adopted for all further calculations. For the fAGN population this implies a contribution of $CXB_{\mathrm{fAGN}} = 9\times10^{-16}\,\mathrm{W\,m^{-2}\,deg^{-2}}$, while assuming an average redshift of $z_{\mathrm{fAGN}} = 4$.

This is in reasonable agreement with the CXB measurements by Moretti et al. (2003), who give a total soft (0.5–2.0 keV) CXB of $75.3\times10^{-16}\,\mathrm{W\,m^{-2}\,deg^{-2}}$ with a $3.5\times10^{-16}\ \mathrm{W\,m^{-2}\,deg^{-2}}$ component (4.6%) not accounted for by either point sources, diffuse emission, or scattering. We note that CXB_{fAGN} is an upper limit to the contribution of fAGN to the CXB. First, because the adopted mass of their central SMBH is an upper limit, and second, no dust extinction of the X-ray emission (predominantly affecting the soft band) was considered, which would result in the absorption of X-ray flux and re-emission at longer wavelengths. To calculate the contribution of fAGN to the hard CXB, one first needs to integrate the Sazonov et al. (2004) template spectrum in the observer's frame 2.0–10 keV range to obtain a fraction for the amount of energy radiated at these wavelengths. We derived a fraction of $f_{\mathrm{X}} = 0.1$, which we then used in Eq. (5) to calculate the hard band X-ray flux in the same manner as done above for the soft band. This results in a contribution of fAGN to the 2.0–10 keV region of the CXB of $3\times10^{-15}\,\mathrm{W\,m^{-2}\,deg^{-2}}$, which is about 18% of the total value in this band given by Moretti et al. (2003). These authors also give 88.8% as the fraction of resolved point-like and extended sources contributing to the hard fraction of the CXB, implying an unresolved component of 11.2%. Hence in the hard band the fAGN population is also able to accurately account for the unresolved fraction of the CXB. However, even though our estimates match other observations and predictions, these calculations should be understood only as a rough estimate of the IFRS number densities and hence fAGN population contributing to the CXB.

4.3. ... on structure formation

The presence of a population of AGN-driven objects of which at least a fraction (up to 50%) is likely to be located at very high redshifts ($z > 5$) places several constraints on the formation scenario of SMBHs shortly after the Big Bang. The Millennium Simulation (Springel et al. 2005), to date the largest cosmological simulation probing ΛCDM cosmology, contains only one massive ($M_{\mathrm{DM-halo}} = 5.5\times10^{12}\,M_\odot$) halo at $z = 6.2$, which is a candidate for a quasar sufficiently bright to be observed by the SDSS. The SMBH mass density at $z = 6$ of $\sim10^{-9}\,M_\odot\,\mathrm{Mpc^{-3}}$ derived from this simulation is therefore several orders of magnitude lower than the mass density we extrapolate from our fAGN (Eq. (4)). We note, however, that bright quasars are still very rare objects that can be treated as statistical "spikes" in the primordial density profile, thus do not very much affect current theories concerning structure formation. Given the very low number density of these bright SDSS quasars (about 0.012 deg^{-2}, see Schneider et al. 2010) or the powerful high redshift radio sources (which need to be selected from all-sky radio surveys, see Seymour et al. 2007), we point out that IFRS or fAGN, respectively, can play an important role just because of their abundance of several tens to several hundred per square degree.

One can also compare the mass densities to models of SMBH formation. Bromley et al. (2004) assert that major mergers account for most of the high-z SMBHs. Their approach yields a close match to our mass density, in particular when their simulation scenario G is considered, where the probability of forming a seed black hole during a merger event is less than unity and the fraction of halo gas accreted onto the black hole is constant. This scenario yields a mass density of $\sim10^3\,M_\odot\,\mathrm{Mpc^{-3}}$ when SMBHs with $10^8\,M_\odot$ at $z = 6$ are considered. Since not all fAGN are likely to be located at such high redshifts, their model variant B, in which the halo gas accretion fraction is proportional to the halo virial velocity squared, is also promising, and yields a mass density of $\sim5\times10^2\,M_\odot\,\mathrm{Mpc^{-3}}$. Another attempt to model SMBH properties at such high redshifts was carried out by Tanaka & Haiman (2009) using both accretion and merger scenarios. They find that to produce sufficient high-mass SMBHs that power the most luminous SDSS quasars ($\geq10^9\,M_\odot$), their models yield a mass density of $10^5\,M_\odot\,\mathrm{Mpc^{-3}}$ for SMBHs with masses around $10^8\,M_\odot$, emphasising that this is too large by a factor of 100 to 1000. Hence, their estimate for these $10^8\,M_\odot$ SMBHs is also of the order $10^2\,M_\odot\,\mathrm{Mpc^{-3}}$.

We conclude that a non-negligible fraction of lower-mass SMBHs at the highest redshifts can place constraints on structure formation after the Big Bang – in particular considering SMBH growth models connected to the build-up of galaxies. Most of these theoretical frameworks focus only on the high-mass SMBHs necessary to power the most luminous quasars. Present observations of lower-mass SMBHs are not possible using currently available instruments with reasonable integration times, but radio observations can play a crucial role in investing the effects of black holes on various scales in the early universe.

5. Summary, conclusions, and outlook

We have investigated the implications of infrared-faint radio sources (IFRS) being high-redshift AGN. We have drawn the consequences for AGN number counts and SMBH mass densities, the cosmic X-ray background (CXB), and theoretical models of structure formation after the Big Bang. Our main results are:

1. The IFRS surface density, which is strongly tied to the sensitivity limit of the parent radio survey (Fig. 2), can be extrapolated to a "zero noise" survey, yielding an intrinsic surface density of $(30.8\pm15.0)\,\mathrm{deg^{-2}}$. Previous work indicates that IFRS are AGN-driven objects at high redshifts, hence this surface density can be converted to a space density of $n_{\mathrm{IFRS}} = 1.44\times10^{-6}\,\mathrm{Mpc^{-3}}$, if they are in the redshift range $3 \leq z \leq 6$.

2. Correcting for the finding that ∼10% of all AGN are radio-loud, a population of high-redshift AGN ("fAGN") is traced by IFRS, of which 10% are only visible in the radio. Almost no IR, optical, and X-ray detections have been made so far, which can be used to constrain the lower-luminosity population of high-redshift AGN. Comparing the number density of these fAGN, $n_{\rm fAGN} = 1.44 \times 10^{-5}\,{\rm Mpc}^{-3}$, to number densities of low-luminous AGN obtained in the X-ray regime, we found them to be in good agreement ($n_{\rm X-ray} = 2 \times 10^{-5}\,{\rm Mpc}^{-3}$). For the most distant AGN ($z > 4$), the X-ray-derived lower limit of 30–150 $\deg^{-2}$ is more than doubled by the fAGN, which have a surface density of the order of 310 $\deg^{-2}$.
3. We found that fAGN can account for the missing unresolved components in both the soft (0.5–2.0 keV) and hard (2.0–10 keV) band of the CXB. Our estimates yield $CBX_{\rm fAGN,soft} = 9 \times 10^{-16}\,{\rm W\,m^{-2}\,deg^{-2}}$ and $CBX_{\rm fAGN,hard} = 3 \times 10^{-15}\,{\rm W\,m^{-2}\,deg^{-2}}$. These values represent 9% of the soft CXB component (cf. to ∼4.6% assumed to represent the missing unresolved fraction), and 18% of the hard CXB component (cf. to ∼11.2% regarded as the missing unresolved fraction).
4. The existence of a non-negligible fraction of lower-mass SMBHs at such high redshifts is in good agreement with recent cosmological simulations, favouring a formation scenario for early SMBHs based on halo gas accretion as well as major mergers. Only considering statistical "spikes" in the primordial density fluctuations as the ancestors of the SMBH population in the early universe is insufficient. Our findings conflict with those of older simulations that attribute the low number of SMBHs to the low number of high-redshift quasars known, an argument taht has become invalid.

Future observations of the IFRS population will constrain the nature and thus the astrophysical significance of these objects. In particular, sub-mm observatories such as ESO's ALMA array or the *Herschel* Space Observatory will be able to provide constraints on the MIR/FIR emission of IFRS. They will clarify whether the IFRS population consists predominantly of highly obscured type II AGN, or IFRS in general have flatter SEDs without any distinct far-infrared bump produced by dust. Corresponding deep *Herschel* observations have already been awarded time and will be executed in the forthcoming observational period. They will place constraints on the star formation history of the universe by estimating dust masses for objects at redshifts potentially as high as $z = 6$.

Acknowledgements. We thank our anonymous referee for his helpful comments that improved this paper very much in terms of clarity and readability.
This research has made use of the NASA/IPAC Extragalactic Database (NED) which is operated by the Jet Propulsion Laboratory, California Institute of Technology, under contract with the National Aeronautics and Space Administration.

References

Alonso-Herrero, A., Colina, L., Packham, C., et al. 2006, ApJ, 652, L83
Appleton, P. N., Fadda, D. T., Marleau, F. R., et al. 2004, ApJS, 154, 147
Athreya, R. M., & Kapahi, V. K. 1998, J. Astrophys. Astron., 19, 63
Bauer, F. E., Alexander, D. M., Brandt, W. N., et al. 2004, AJ, 128, 2048
Bell, E. F. 2003, ApJ, 586, 794
Brandt, W. N., & Hasinger, G. 2005, ARA&A, 43, 827
Bromley, J. M., Somerville, R. S., & Fabian, A. C. 2004, MNRAS, 350, 456
Brusa, M., Comastri, A., Gilli, R., et al. 2009, ApJ, 693, 8
Calzetti, D., Armus, L., Bohlin, R. C., et al. 2000, ApJ, 533, 682
Cappelluti, N., Hasinger, G., Brusa, M., et al. 2007, ApJS, 172, 341
Condon, J. J., Cotton, W. D., Yin, Q. F., et al. 2003, AJ, 125, 2411
Degraf, C., Di Matteo, T., & Springel, V. 2010, MNRAS, 402, 1927
Dietrich, M., & Hamann, F. 2004, ApJ, 611, 761
Dijkstra, M., Haiman, Z., & Loeb, A. 2004, ApJ, 613, 646
Fan, X. 2009, in ASP Conf. Ser. 408, ed. W. Wang, Z. Yang, Z. Luo, & Z. Chen, 439
Fan, X., Strauss, M. A., Schneider, D. P., et al. 2003, AJ, 125, 1649
Fazio, G. G., Hora, J. L., Allen, L. E., et al. 2004, ApJS, 154, 10
Fine, S., Croom, S. M., Hopkins, P. F., et al. 2008, MNRAS, 390, 1413
Garn, T., & Alexander, P. 2008, MNRAS, 391, 1000
Gawiser, E., van Dokkum, P. G., Herrera, D., et al. 2006, ApJS, 162, 1
Giavalisco, M., Ferguson, H. C., Koekemoer, A. M., et al. 2004, ApJ, 600, L93
Gilli, R., Comastri, A., & Hasinger, G. 2007, A&A, 463, 79
Hasinger, G., Miyaji, T., & Schmidt, M. 2005, A&A, 441, 417
Huynh, M. T., Norris, R. P., Siana, B., & Middelberg, E. 2010, ApJ, 710, 698
Ibar, E., Ivison, R. J., Biggs, A. D., et al. 2009, MNRAS, 397, 281
Jiang, L., Fan, X., Ivezić, Ž., et al. 2007, ApJ, 656, 680
Lacy, M., Wilson, G., Masci, F., et al. 2005, ApJS, 161, 41
Lonsdale, C. J., Smith, H. E., Rowan-Robinson, M., et al. 2003, PASP, 115, 897
Luo, B., Bauer, F. E., Brandt, W. N., et al. 2008, ApJS, 179, 19
Middelberg, E., Norris, R. P., Cornwell, T. J., et al. 2008a, AJ, 135, 1276
Middelberg, E., Norris, R. P., Tingay, S., et al. 2008b, A&A, 491, 435
Middelberg, E., Norris, R. P., Hales, C. A., et al. 2011, A&A, 526, A8
Moretti, A., Campana, S., Lazzati, D., & Tagliaferri, G. 2003, ApJ, 588, 696
Mushotzky, R. 2004, in Supermassive Black Holes in the Distant Universe, ed. A. J. Barger, Astrophys. Space Sci. Lib., 308, 53
Norris, R. P., Afonso, J., Appleton, P. N., et al. 2006, AJ, 132, 2409
Norris, R. P., Tingay, S., Phillips, C., et al. 2007, MNRAS, 378, 1434
Norris, R. P., Afonso, J., Cava, A., et al. 2011, ApJ, accepted
Owen, F. N., & Morrison, G. E. 2008, AJ, 136, 1889
Puccetti, S., Fiore, F., D'Elia, V., et al. 2006, A&A, 457, 501
Rix, H., Barden, M., Beckwith, S. V. W., et al. 2004, ApJS, 152, 163
Sanders, D. B., Salvato, M., Aussel, H., et al. 2007, ApJS, 172, 86
Sazonov, S. Y., Ostriker, J. P., & Sunyaev, R. A. 2004, MNRAS, 347, 144
Schinnerer, E., Smolčić, V., Carilli, C. L., et al. 2007, ApJS, 172, 46
Schneider, D. P., Richards, G. T., Hall, P. B., et al. 2010, AJ, 139, 2360
Seymour, N., Stern, D., De Breuck, C., et al. 2007, ApJS, 171, 353
Snellen, I. A. G., & Best, P. N. 2001, MNRAS, 328, 897
Somerville, R. S., Lee, K., Ferguson, H. C., et al. 2004, ApJ, 600, L171
Springel, V., White, S. D. M., Jenkins, A., et al. 2005, Nature, 435, 629
Tanaka, T., & Haiman, Z. 2009, ApJ, 696, 1798
Vestergaard, M., & Osmer, P. S. 2009, ApJ, 699, 800
Vestergaard, M., Fan, X., Tremonti, C. A., Osmer, P. S., & Richards, G. T. 2008, ApJ, 674, L1
Willott, C. J., Albert, L., Arzoumanian, D., et al. 2010, AJ, 140, 546
Wright, E. L. 2006, PASP, 118, 1711